HSA-hijacking nanobinders built on bioresponsive prodrugs for combined cancer chemoimmunotherapy

Matilde Tubertini[a,‡], Luca Menilli[b,‡], Celeste Milani[b,‡], Cecilia Martini[a], Maria Luisa Navacchia[a], Marta Nugnes[c], Manuela Bartolini[c], Marina Naldi[c], Daniele Tedesco[a], Elisa Martella[a], Andrea Guerrini[a], Claudia Ferroni[a], Francesca Moret[b,] and Greta Varchi[a,*]*

[a]Institute for Organic Synthesis and Photoreactivity (ISOF), National Research Council of Italy (CNR), Via P. Gobetti 101, 40129 Bologna, Italy.

[b]Department of Biology (DiBio), University of Padova, Via U. Bassi 58/B, 35100 Padova, Italy.

[c]Department of Pharmacy and Biotechnology (FaBiT), University of Bologna, Via Belmeloro 6, 40126 Bologna, Italy.

KEYWORDS Prodrugs, chemoimmuno therapy, endogenous human serum albumin, carrier-free nanoparticles, truncated Evans Blue, triple-negative breast cancer

ABSTRACT Triple-negative breast cancer (TNBC) is an aggressive subtype of breast cancer still lacking effective treatment options. Chemotherapy in combination with immunotherapy can restrict tumor progression and repolarize the tumor microenvironment towards an anti-tumor milieu, improving clinical outcome in TNBC patients. The chemotherapeutic drug paclitaxel had been shown to induce immunogenic cell death (ICD), whereas inhibitors of the indoleamine 2,3-

dioxygenase 1 (IDO1), whose expression is shared in immune regulatory and tumor cells, have been revealed to enhance the anti-tumor immune response. However, poor bioavailability and pharmacokinetic, off-target effects and hurdles in achieving therapeutic drug concentrations at the target tissue often limit the effectiveness of combination therapies. This work describes the development of novel biomimetic and carrier-free nanobinders (NB) loaded with both paclitaxel and the IDO1 inhibitor NLG919 in the form of bioresponsive prodrugs, and capable of hijacking human serum albumin (HSA). A fine tuning of the preparation conditions allowed to identify NB@5 as the best performing prodrugs-based nanoformulation. Our data show that NB@5 effectively binds with HSA, demonstrating its protective role in the controlled release of drugs *in vitro* and suggesting that NB could exploit the protein as the endogenous vehicle for targeted delivery to the tumor site. Our study successfully demonstrates that the drugs encapsulated within the nanobinders are preferentially released under the altered redox conditions commonly found in the tumor microenvironment, thereby inducing cell death, promoting ICD, and inhibiting IDO1. This study highlights the potential of prodrugs-based nanobinders as a promising avenue for the targeted chemoimmunotherapy of TNBC.

1. INTRODUCTION

Although cancer therapy has made significant progresses in recent years, certain solid tumors or their most aggressive subtypes still lack effective treatment options. One such example is triple-negative breast cancer (TNBC), accounting for 15-20% of all breast cancers. TNBC is characterized by the absence of estrogen, progesterone, and human epidermal growth factor 2 receptors, and it is associated with high rates of distant recurrence and reduced overall survival.[1] In light of the limited efficacy of current treatments, significant efforts have been undertaken in recent years to expand therapeutic options for TNBC patients.[2,3] Over the past decade, a substantial

body of evidence has underscored the crucial role of the immune system in shaping the disease course.[4] Tumor-infiltrating lymphocytes (TILs) are widely acknowledged as a reliable indicators of favorable prognosis in both adjuvant and neoadjuvant treatments.[5,6] Alongside TILs, the expression of immune evasion molecules in the TME, like programmed death-ligand 1 (PD-L1) and indoleamine-2,3-dioxygenase enzyme 1 (IDO1), has also been demonstrated to negatively influence TNBC prognosis.[7–9] In particular, the cytotoxic killing ability of TILs may be limited by the overexpression of IDO1 due to its interference with immune metabolism.[10–12] IDO1 catalyzes the first and rate-limiting step of the kynurenine (Kyn) pathway, where the essential amino acid L-tryptophan (Trp) is converted into the immunosuppressive metabolite L-Kyn. The effect of this conversion is two-fold: Trp depletion induces apoptosis in T cells through the action of the mammalian target of rapamycin complex 1 (mTORC1) regulatory protein,[13] while increased levels of Kyn activate the aryl hydrocarbon receptor (AHR), a transcription factor responsible for the differentiation of effector $CD4^+$ cells into T_{reg} cells.[14] Therefore, IDO1 inhibition has been revealed as a promising approach to rewire immune surveillance towards cancer cells.[15–17]

In parallel, recent studies have demonstrated that specific chemotherapeutic agents drugs, such as doxorubicin, camptothecin, oxaliplatin and paclitaxel (Ptx) can induce immunogenic cell death (ICD).[18] During ICD, dying cancer cells release damage-associated molecular patterns (DAMPs) and danger signals, such as calreticulin (CRT), adenosine 5′-triphosphate (ATP) and the high-mobility group box 1 protein (HMGB1), which collectively recruit phagocytic cells and activate the immune system at the tumor site. Additionally, ICD is characterized by the exposure of tumor antigens on the surface of dying cancer cells, which can be taken up by antigen-presenting cells to stimulate T cell response.[19] ICD is of great interest in cancer immunotherapy, as it can enhance the effectiveness of immune checkpoint inhibitors, such as IDO1 inhibitors, by priming the

immune system to recognize and attack cancer cells.[20] Therefore, inducing ICD and relieving IDO1 immunosuppression by combining drugs capable of simultaneously reaching the TME in an appropriate ratio is expected to achieve potent antitumor efficacy in TNBC.

Approaching combination therapy by including multiple drugs within a single entity represents a meaningful way to reduce unwanted toxicities, ensure comparable pharmacokinetic and achieve an improved ratiometric delivery of drugs at the tumor site.[12] In this context, carrier-free drug delivery systems have gained much attention thanks to their unique advantages over carrier-based ones, such as high drug payload and no carrier-induced toxicity.[21]

In addition, exploiting endogenous human serum albumin (HSA) binding is a valuable option to achieve tumor targeting and improve the pharmacokinetic profile of drugs and nanosystems.[22] As a major source of energy and amino acids, HSA is actively recruited into the TME allowing enhanced accumulation in tumor tissues compared to normal ones.[23] Hence, endogenous HSA can serve as a valuable carrier for targeted drug delivery to tumors by utilizing albumin-binding moieties, enabling the biomimetic delivery of drugs to tumor cells.[24,25] Several studies have shown that the attachment of drugs or molecular conjugates to HSA significantly prolongs their circulation time and decreases their clearance from the reticuloendothelial system (RES), thus promoting accumulation and retention at the tumor site.[26]

Given these considerations, this study introduces a unique and pioneering biomimetic nanosystem that encompasses two primary breakthrough components: i) the design and synthesis of novel non-covalent HSA-binding amphiphilic prodrugs of the cytotoxic drug Ptx and of the IDO1 inhibitor NLG919 (Nlg) and (ii) the subsequent formulation of these prodrugs into HSA-binding and carrier-free nanobinders (NBs). It is noteworthy that the strategic use of prodrugs

assumes particular significance, as it ensures a more precise control over drug release, imparts amphiphilicity, and enhances NBs stability within physiological contexts.

Our main objective is to demonstrate, through *in vitro* two- and three-dimensional models of TNBC, that HSA-binding prodrugs and their corresponding NBs can augment the antitumor cytotoxicity and the ICD effect of Ptx while counteracting the immunosuppressive effects induced by IDO1 overexpression. This extensive and exploratory study lays the foundation for further preclinical validation of carrier-free and biomimetic NBs as a potential therapeutic option for treating TNBC and all solid tumors characterized by increased IDO1 expression.[15]

2. EXPERIMENTAL SECTION

2.1. Materials chemistry

Pure paclitaxel (Ptx) was kindly provided by Indena SpA (Italy). NLG919 (Nlg) was purchased from Zentek Srl (Italy). Unless otherwise stated, all other reagents were purchased from Sigma-Aldrich (Merck, Italy). All reagents were used as obtained from commercial sources unless otherwise indicated; solvents for synthesis were dried over standard drying agents and freshly distilled prior to use. Ultrapure water (uH_2O) was produced using a Sartorius Arium Pro® system. Proton and carbon-13 nuclear magnetic resonance (^{1}H-NMR and ^{13}C-NMR) spectra were recorded on a 500 MHz Agilent DD2 PremiumCompact Plus NMR spectrometer, equipped with a single ADC console and a OneNMR probe, and a 400 MHz Varian Mercury NMR spectrometer, equipped with an AutoSwitchable probe. Deuterated solvents – deuterium oxide (D_2O), methanol-d4 (CD_3OD), chloroform-d ($CDCl_3$), dimethyl sulfoxide-d_6 (DMSO-d_6), acetone-d_6 – were purchased from Eurisotop (France) and used as specified for each compound. 1H chemical shifts values (δ, in ppm) are referenced to the residual non-deuterated components of the NMR solvents. ESI-MS data were acquired on a TSQ Quantum Access Max Triple Quadrupole mass

spectrometer. Flash chromatography was performed on a Teledyne Isco CombiFlash Rf 200 system using RediSep Rf normal-phase silica gel flash columns (230–400 mesh). Thin-layer chromatography (TLC) was performed on plastic plates coated with silica gel 60 and fluorescent indicator F254. All compounds tested in biological assays were >95% pure, as determined by high-performance liquid chromatography analysis with ultraviolet detection (HPLC–UV) performed on a Shimadzu Nexera XR UHPLC system equipped with a LC-40D XR pump, a SIL-40C XR autosampler, a DGU-405 degassing unit, a CTO-40S column oven and a SPD-M40 photodiode array (PDA) detector. The purity of intermediates was >90%, unless otherwise stated. Solvents and reagents for analytical studies – methanol (MeOH), ethanol (EtOH), acetonitrile (ACN), trifluoroacetic acid (TFA), ammonium acetate (NH_4OAc), acetic acid (AcOH), dimethyl sulfoxide (DMSO) – were of HPLC grade or higher.

All synthetic procedures and compounds characterization including NMR spectra (Figures S1-S17) are reported in the supporting information section (pages 3 – 21).

2.2. HSA binding affinity

Surface plasmon resonance (SPR) analysis was performed using a Biacore X100 (GE Healthcare, Italy). Binding affinities (expressed as dissociation constants, KD) were determined by single-cycle analysis using a functionalized CM5 sensor. In both flow cells, an anti-human serum albumin antibody (polyclonal anti-human albumin antibody, Sigma-Aldrich Merck) was immobilized by amine coupling using an Amine Coupling kit (GE Healthcare); the functionalized sensor chip was then used to bind HSA (96%, essentially fatty acid free, product code A1887; Sigma-Aldrich, Merck, Italy) by immunocapturing. Analyses were performed using a single-cycle kinetics approach: at each single-cycle analysis, a 50 µM HSA solution was flowed on the surface of the active cell at a flow rate of 5 µL/min for 840 s to allow HSA immunocapturing. tEB and

pMAC1 solutions were prepared at concentrations of 0.781, 1.56, 3.12, 6.25 and 12.5 µM while pMAC2 and nMAC were prepared at concentrations of 1.56, 3.12, 6.25, 12.5 and 25 µM in phosphate buffered saline (PBS) pH 7.4 with 0.05% polysorbate 20 and 2% DMSO. Analysis was performed at a flow rate of 30 µL/min. Each analyte solution was allowed to interact with HSA for 120 s. Two subsequent regeneration steps were performed at the end of the cycle by injecting a 100 mM glycine hydrochloride (Gly) solution and a 50 mM sodium hydroxide (NaOH) solution at a flow rate of 10 µL/min for 40 s for surface regeneration. The SPR sensorgrams were corrected by a double referencing procedure and globally fitted using a 1:1 binding model. KD values were calculated using the Biacore X100 Evaluation Software version 2.0.1 in affinity mode (GE Healthcare). All SPR experiments were performed in duplicate, and binding affinities for each analyte were averaged over the two experiments.

2.3. Prodrug stability

The stability of prodrugs (pMal, pMAC1, pMAC2, nMAC) was determined on 10 µM samples prepared by diluting stock solutions (1 mM in DMSO) to 40 µM in EtOH before addition of PBS pH 7.4 (final solvent: PBS/EtOH 75:25, v/v). Four different concentrations of dithiothreitol (DTT) were used to test the sensitivity of prodrugs towards the redox potential of the environment (0 mM, 0.2 mM, 1 mM, 10 mM). The effect of HSA on stability was also evaluated on equimolar mixtures (10 µM) of protein and prodrugs and tested under the same redox conditions. Two independent samples were prepared for each condition and submitted without further purification to HPLC-UV analysis, which was carried out on the Shimadzu Nexera XR system with a Phenomenex Jupiter C4 column (150×2.0 mm I.D., 5 µm particle size, 300 Å pore size) using an injection volume of 20 µL. Gradient elution was achieved by mixing mobile phases A (TFA 0.1% in uH_2O, v/v) and B (TFA 0.1% in ACN, v/v) at a constant flow rate of 0.5 mL/min, according to the following time

program: 0 min, 20% B; 0.50 min, 20% B; 2.75 min, 35% B; 5.75 min, 45% B; 7.25 min, 55% B; 9.30 min, 55% B; 9.50 min, 20% B, 13.33 min, 20% B. Column oven and autosampler temperatures were set to 40 °C and 20 °C, respectively. Chromatograms at the relevant detection wavelengths (556 nm for pMAC1, pMAC2 and nMAC; 392 nm for pMal) were extracted from PDA data (600–200 nm). Analytes were identified based on their retention times (t_R) and PDA-extracted UV spectra (Figure S18, ESI). The quantities of unreacted prodrugs in the presence and absence of HSA were monitored at four different time steps after sample preparation (10 min, 1 h, 2 h, 3 h) by summing the peak areas of pMal (t_R = 10.9 min), pMAC1 (t_R = 10.2 min), pMAC2 (t_R = 9.8 min) or nMAC (t_R = 6.0 min) to that of HSA-bound prodrugs (t_R = 6.7 min for HSA). Prodrug stabilities (% m/m) as a function of reaction time were finally derived for each redox condition from the cumulative peak areas of prodrugs relative to those obtained in the absence of DTT at the initial time step of the assay (Figure S19, ESI).

2.4. Nanobinders preparation and characterization

For single-component micelles preparation, e.g., @pMal and @NlgD, uH_2O was added to a solution of prodrugs dissolved in EtOH under vigorous stirring. After stirring at room temperature (r.t.) for 2 h, the suspension was purified by ultrafiltration (UF) with a regenerated cellulose centrifugal filter (MWCO:10 kDa; Amicon Ultra, Millipore, Merck, Italy), centrifuged and resuspended with uH_2O followed by vortexing at 8000 rpm (5 min) and at 4000 rpm (2 min) (3x). All experimental details on prodrugs stock solutions and relative ratios are reported in Table S3.

Multi-component micelles including fluorescently labelled NBs, e.g., @pMal-NlgD, NBs and f-NBs, were prepared by dissolving the bioresponsive prodrug(s) and the Nile Red dye (for fluorescent NBs) in *N*,*N*-dimethylformamide (DMF) or EtOH and the obtained solution was slowly added to uH_2O under vigorous stirring to form micelles. After stirring at r.t. for 2 h, the suspensions

were purified as previously described for single component micelles. All experimental details on prodrugs and Nile Red stock solutions and relative ratios are reported in Tables S4 and S5.

The hydrodynamic diameter and polydispersity index (PDI) of micelles were determined by dynamic light scattering (DLS) at 25°C using a NanoBrook Omni Particle Size Analyzer (Brookhaven Instruments Corporation, USA) equipped with a 35 mW red diode laser (nominal wavelength 640 nm). The measurements were performed on samples prepared by diluting 50 μL of micelles' solution in 1,6 mL of uH_2O (representative concentration = 60 μg/mL). Electrophoretic mobility, i.e., ζ-potential, was measured at 25 ◦C using the DLS instrument.

Stability studies on micelles suspensions (50 μg/mL) were performed over time in PBS pH 7.4 (37 °C, 24 h) with or without HSA (35 mg/mL) and fetal bovine serum (FBS; 10% v/v). In a typical experiment, 0.2 mL of micelles suspension (2.5 mg/mL) were diluted with 1.8 mL of the selected stability medium, while maintaining them at 37 °C. Changes in particles' size distribution were monitored by DLS. NB morphology was analyzed by transmission electron microscopy (TEM). Sample micelles (0.1 mg/mL), pre-incubated or not with HSA (10:1, m/m), were dispensed as a drop on a carbon-coated nickel grid and after 20 min, any excess of the solution was absorbed by filter paper. The nanoformulation was subsequently observed with a Jeol Jem-1011 transmission electron microscope (Jeol Jem, Peabody, USA).

2.5. Drug release

The release of drugs from NB@5 was evaluated by equilibrium dialysis and HPLC-UV analysis, which was performed on the Shimadzu Nexera XR system with a Phenomenex Kinetex C18 column (150×4.6 mm I.D., 5 μm particle size, 100 Å pore size) using an injection volume of 50 μL. Gradient elution was achieved by mixing mobile phases A (NH_4OAc 20 mM in uH_2O, pH 5.1 buffer with AcOH) and B (NH_4OAc 20 mM in MeOH) at a constant flow rate of 1.0 mL/min,

according to the following time program: 0 min, 50% B; 2.50 min, 50% B; 6.50 min, 90% B; 9.00 min, 90% B; 9.10 min, 50% B; 13.33 min, 50% B. Column oven and autosampler temperatures were set to 40 °C and 10 °C, respectively. Chromatograms at the relevant detection wavelengths (228 nm for Ptx, 271 nm for Nlg) were extracted from PDA data (600–200 nm). NB@5 suspensions were prepared in uH_2O at a nominal concentration of 202.4 µg/mL, equivalent to a Ptx concentration of 50 µg/mL after complete reaction of pMAC2. Samples for dialysis (250 µL) were then loaded into Pur-A-Lyzer Mini dialysis devices (MWCO: 12 kDa) and dialyzed against 2.5 mL of release medium (PBS/EtOH 75:25 v/v; total volume: 2.75 mL) for 48 h at 37 °C; three different DTT concentrations (0 mM, 1 mM, 10 mM) were tested to assess the sensitivity of drug release towards the redox potential of the environment. During dialysis, aliquots (150 µL) were sampled from release media at 14 time points (one every 20 min from 5 min to 85 min, one every hour from 2 h to 7 h, then 24 h, 28 h and 48 h), replaced with the same volume of fresh medium and submitted to HPLC-UV analysis with duplicate injections. The exact contents of Ptx and Nlg in NB@5 suspensions were determined after a 1:10 dilution, achieved by sequential addition of ACN (5 volumes) and DTT (50 mM in uH_2O; 4 volumes), yielding samples (20.24 µg/mL) dissolved in a solution of DTT 20 mM in uH_2O/ACN 50:50 (v/v); sonication cycles (10 min) were performed after each dilution step to facilitate the full solubilization of prodrugs. The resulting samples (n = 3) were incubated at 45 °C for 3 h to drive the drug release reaction from prodrugs to completion, then submitted to HPLC-UV analysis with duplicate injections. The released quantities of Ptx and Nlg at each time point were determined from the cumulative peak areas for the main stereoisomers of both drugs (Figure S20) – Ptx (t_R = 7.5 min) and 7-epi-Ptx (t_R = 7.8 min), resulting from the epimerization of Ptx at pH 7.4; (*R*,*S*)/(*S*,*R*)-Nlg (t_R = 7.9 min) and (*S*,*S*)/(*R*,*R*)-Nlg (t_R = 8.1 min) – using calibration curves obtained by linear regression (Table S1

and Figure S21), then expressed as mass fractions (% m/m) relative to their exact contents in NB@5 suspensions (Table S2). Kinetic profiles were derived by plotting mass fractions as a function of dialysis time.

2.6. Cell lines

MDA-MB-468, MDA-MB-231 (human TNBC cells), and MCF10A (human non-malignant breast epithelial) cell lines were purchased from American Type Culture Collection (ATCC, USA). MDA-MB-468 and MDA-MB-231 cells were grown in Dulbecco's Modified Eagle Medium-High Glucose (DMEM-HG) with Glutamax^{TM} supplemented with 10% heat-inactivated FBS and antibiotics (100 U/mL streptomycin, 100 µg/mL penicillin G). MCF10A cells were cultured in DMEM/F12 medium supplemented with 5% horse serum, 20 ng/mL epidermal growth factor, 0.5 mg/mL hydrocortisone, 100 ng/mL cholera toxin, 10 µg/mL insulin, and antibiotics. Cells were maintained at 37 °C under a humidified atmosphere, containing 5% carbon dioxide (CO_2). Cell culture media and supplements were purchased from Life Technologies (Italy), while sterile plasticware was purchased from Falcon (Corning, USA).

2.7. *In vitro* studies on TNBC cells monolayers

2.7.1. Cytotoxicity of prodrugs and nanobinders

The cytotoxic effects of synthetized Ptx prodrugs, NB and controls (e.g., reference drugs) in TNBC cells and in the non-malignant counterpart were assessed using CellTiter 96® AQueous One Solution Cell Proliferation Assay (MTS, Promega, Italy). MDA-MB-468 (8×10^3 cells/well), MDA-MB-231 (8×10^3 cells/well) and MCF-10A (6×10^3 cells/well) cells were seeded in 96-well plates and allowed to growth for 24 h. Cells were treated for 24 or 48 h with increasing concentrations of Ptx-based prodrugs or NB diluted in culture media. For the MTS assay, the medium was replaced with 100 µL of serum-free medium and 20 µL of the CellTiter 96® reagent.

After 60-90 min, depending on the cell line, the absorbance at 492 nm was measured with a Multiskan Go (Thermo Fischer Scientific, USA) plate reader and cell viability was expressed as a function of absorbance relative to that of control cells (considered as 100% viability). Cell viability data were elaborated with the software GraphPad Prism 9.5 to obtain dose-effect curves and calculate the half maximal inhibitory concentration value (IC_{50}) of each tested compound. To assess the effectiveness of NB in a simulated TME (*i.e.,* different reducing conditions), the viability assay was performed in the presence of DTT (10 μM and 10 mM) and HSA (NB@5/HSA 1:10 m/m). Briefly, NB@5 were incubated with HSA for 30 min at 37 °C and for further 2 h in the presence of DTT. Cells were then treated for 48 h with pre-treated NB@5 at the corresponding concentrations of Ptx of 0.01 μM and 0.1 μM.

2.7.2. Kynurenine assay: IDO1 inhibition in vitro

The inhibitory activity on IDO1 of Nlg, Nlg prodrugs and Nlg-containing NBs was assessed by measuring kynurenine content in cell culture media. MDA-MB-468 cells (8×10^3 cells/well) were seeded into 96-well plate and allowed to grow overnight. Cells were stimulated with 50 ng/mL of recombinant human interferon-γ (IFN-γ; Life Technologies, Italy) to induce the expression of IDO1 and simultaneously treated with three concentrations of Nlg formulations (e.g., 0.1, 1 and 10 μM). After incubation (24 h), 140 μL of the supernatant from each well were transferred to a new 96-well plate and mixed with 50 μL of 30% trichloroacetic acid. The plate was incubated for 30 min at 50 °C to facilitate proteins precipitation and then centrifuged at 2500 rpm. Then, 100 μL of the resulting supernatants were collected in a new plate and mixed with an equal volume of Ehrlich reagent (2% p-dimethylaminobenzaldehyde in glacial AcOH, w/v). After 10 min of incubation, the absorbance at 490 nm was determined using Multiskan GO microplate reader.

2.7.3. Immunogenic cell death (ICD)

The induction of immunogenic cell death by Ptx-containing formulations on the MDA-MB-468 and MDA-MB-231 cell lines was assessed by analyzing CRT exposure on the plasma membrane, migration of HMGB1 from the nucleus to the cytoplasm and ATP release. CRT exposure and HMGB1 migration were detected by immunofluorescence. Briefly, 5×10^4 cells were seeded on 4-well chamber slides (Falcon, USA) and grown overnight at 37 °C in in a humidified environment with 5% CO_2. Cells were treated with 0.1 and 1 μM of Ptx-containing formulations and further incubated for 12 h. Cells were then washed with ice-cold PBS twice, fixed with 4% paraformaldehyde for 15 min at RT and permeabilized with 0.1% Triton X-100 for 10 min at r.t. (this last step was done only for HMGB1 detection). Cells were then blocked using a solution containing 2% HSA and 20 mg/mL Gly for 1 h at 37 °C, prior to immunolabeling with rabbit anti-CRT-Alexafluor 488 (1:500) or anti-HMGB1-Alexafluor 488 (1:250) antibodies overnight at 4 °C. Both antibodies are purchased by Abcam. After three washes with PBS, cell nuclei were stained with Hoechst 33342. The slides were then further washed three times with PBS and sealed with VectaShield Plus mounting medium (VectorLabs, USA). Cells were imaged with a ZEISS LSM 900 with Airyscan 2 confocal microscope and, subsequently, were analyzed with the software Fiji. Briefly, for each cell was defined the region of interest (ROI) and the integrated density, that correspond to the fluorescence, was measured. ATP release from cells was measured using the RealTime-Glo™ Extracellular ATP Assay (Promega, Italy) following the manufacturer's specifications. Briefly, 1×10^4 cells were seeded in white 96-well plates with clear bottom and grown for 24 h. The day after, cells were treated with increasing concentration of Ptx-containing formulations and added with RealTime-Glo Extracellular ATP Assay Reagent. Luciferin luminescence was then monitored using Victor 3 multimodal microplate reader (Perkin Elmer, USA).

2.7.4. Intracellular uptake of nanobinders

The hydrophobic fluorophore Nile Red (NR) was loaded in selected NB formulations to assess their internalization by flow cytometry. 8×10^4 MDA-MB-468 cells were seeded in 24-wells plate in complete medium and allowed to growth for 24 h. Cells were then treated for 2 h with NBs (1 μM NR concentration) diluted in culture medium in the absence or in the presence of 10% FBS. At the end of the incubation time, cells were washed twice with Versene solution, detached from the plates with trypsin that was neutralized by the addition of FBS. Cells were centrifuged and resuspended in Versene before measuring NR fluorescence using a BD Fortessa™ X-20 flow cytometer (Becton Dickinson, USA). A blue laser (488 nm) was used to excite the fluorophore and its fluorescence was detected in the PE-Texas Red channel (610/20 filter). For each sample, 10^4 events were acquired and analyzed using the BD FACSDiva 9.0 software.

2.8. *In vitro* studies on TNBC spheroids

2.8.1. Spheroids generation

MDA-MB-468 spheroids were generated into 96-wells ultra-low attachment plates (Nunclon™ Sphera™ U-shaped bottom microplates, Thermo Fischer Scientific, USA) using the liquid overlay-technique. Briefly, 3.5×10^3 cells/well were seeded in DMEM supplemented with 10% FBS and 6 μL/mL of collagen I (BD Biosciences, USA). Immediately after seeding, cells were centrifuged for 3 min at 100×*g* to promote cell aggregation and allowed to grow in the incubator for 4 days at 37 °C under 5% CO_2 before their use in the following experiments.

2.8.2. Cytotoxicity in spheroids

Cell viability reduction in treated spheroids was assessed using the CellTiter-Glo® 3D Cell Viability Assay (Promega Italia), based on the measurement of intracellular ATP content. Four-days-old MDA-MB-468 spheroids were incubated with fresh medium containing 10% FBS and

increasing concentration of prodrugs or NBs for 72 h before measuring viability. For the assay, 100 µL of medium were left in each spheroid well and 100 µL of CellTiter-Glo® 3D reagent was added; the well was incubated at r.t. for 30 min before transferring the 200 µL of sample/wells in a blank 96/well (Perkin Elmer, Waltham, MA, USA). Luminescence was measured with a Perkin Elmer VICTOR™X3 instrument. Cell viability was expressed as a function of luminescence relative to that of control cells (considered as 100% viability).

2.8.3. Kynurenine assay: IDO1 inhibition in vitro

The inhibitory activity on IDO1 of Nlg, Nlg prodrugs and Nlg-containing NBs was assessed by measuring kynurenine content in cell culture media. 3.5×10^3 MDA-MB-468 cells/well were seeded in 96-well Nunclon Sphera 3D plates (Thermo Fisher, Italy) in complete cell culture medium supplemented with collagen I and allowed to grow for 96 h. Spheroids were stimulated with 50 ng/mL of recombinant human interferon-γ (IFN-γ; Life Technologies, Italy) to induce the expression of IDO1 and simultaneously treated with three concentrations of Nlg formulations (e.g., 0.1, 1 and 10 µM). After incubation (48 h), 140 µL of the supernatant from each well were transferred to a new 96-well plate and mixed with 50 µL of 30% trichloroacetic acid. The plate was incubated for 30 min at 50 °C to facilitate proteins precipitation and then centrifuged at 2500 rpm. Then, 100 µL of the resulting supernatants were collected in a new plate and mixed with an equal volume of Ehrlich reagent (2% p-dimethylaminobenzaldehyde in glacial AcOH, w/v). After 10 min of incubation, the absorbance at 490 nm was determined using Multiskan GO microplate reader.

2.9. Statistical analysis.

The data showed in this study are expressed as mean ± SD. All experiments were performed at least twice and carried out in triplicate, unless otherwise stated in the respective legend figure. All

statistical analyses were performed with GraphPad Prism 9.5 (GraphPad; San Diego, CA, USA) using one-way ANOVA test and Tukey's multiple comparison as a post-test for CRT and HMGB1 quantification. Data reported in Figures 4, 6, 8 and 9 were analyzed using the 2-way ANOVA test and Bonferroni's multiple comparison as a post-test. Results were statistically significant for p-values < 0.05 (*p-values< 0.05, ** p-values< 0.01, *** p-values< 0.001 and ****p-values< 0.0001).

3. RESULTS AND DISCUSSION

3.1. Synthesis of bioresponsive and HSA-binding building blocks

We conceived the design and preparation of bioresponsive Modular Affinity Conjugates (MAC, Figure 1) with diverse functionalities. These MACs consist of an HSA-binding ligand (HBL) capable of selectively binding to the protein *in vivo*, along with one or two drug molecules, such as paclitaxel (Ptx) or NLG919 (Nlg), connected *via* a bioresponsive spacer. As the HBL, we selected the truncated Evans Blue dye (tEB, Figure 1 and Scheme S1). tEB maintains the HSA-binding properties of the native EB, and allows for conjugation with other chemical entities thanks to the presence of a free NH_2 terminal group.[27] Instead of exploiting the covalent bonding with Cys34 on HSA, we intentionally focused the design of our systems on the non-covalent tEB ligand to avoid unwanted cross-reactions with Cys and Lys residues on other blood and cell proteins, as well as to overcome the problems posed by lower availability of free Cys34 associated with the elevated oxidative stress present in cancer patients.[28]

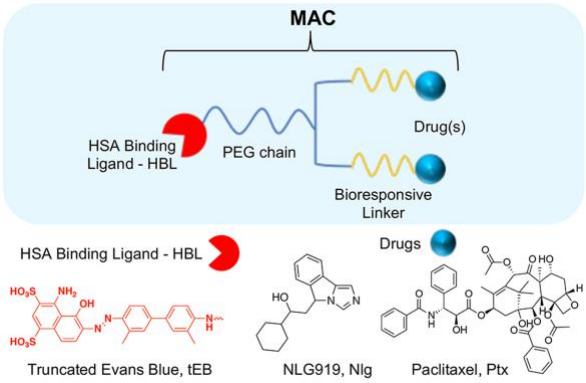

Figure 1. General structure of Modular Affinity Conjugates (MAC) and chemical structures of Nlg, Ptx and tEB.

This work started with the synthesis of the bioresponsive prodrugs required for the fabrication of the corresponding carrier-free nanosystems. Upon exploring different synthetic strategies and considering the challenges of semi-synthetic modifications of natural compounds, such as Ptx, we were able to setup a complex but straightforward process allowing to isolate in good yields derivatives pMAC1 (Scheme 1) and pMAC2 (Scheme 2). The Ptx dimer **1** was synthesized according to an optimized synthetic procedure (Scheme S2) in 85% yield starting from commercially available Ptx. Upon reaction with compound **2** (Supporting Information) in the presence of TCEP·HCl and DIPEA, the corresponding derivative **3** was obtained in 65% yield. The final diazotization reaction afforded the desired compound pMAC1 in 70% yield upon dialysis purification.

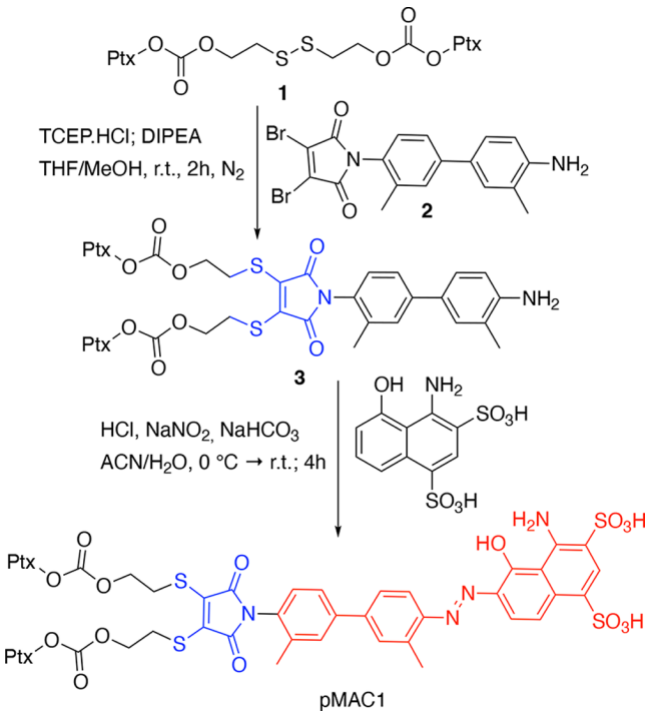

Scheme 1. Synthetic route to pMAC1.

To explore the effect of the linker between the prodrug moiety and the tEB framework on the formation of bioresponsive NBs, a second derivative, namely pMAC2 (Scheme 2) was prepared starting from the Ptx dimer **1**, which was reacted with commercially available 2,3-dibromo maleimide to afford compound pMal in >70% yield. Following a literature procedure applied to different compounds,[29] derivative **4** (Scheme 2) was isolated in quantitative yield and coupled with compound **5** (Scheme S3) to afford **6** in 50% yield. The final diazotization step allowed to isolate the target compound pMAC2 in quantitative yield upon dialysis purification.

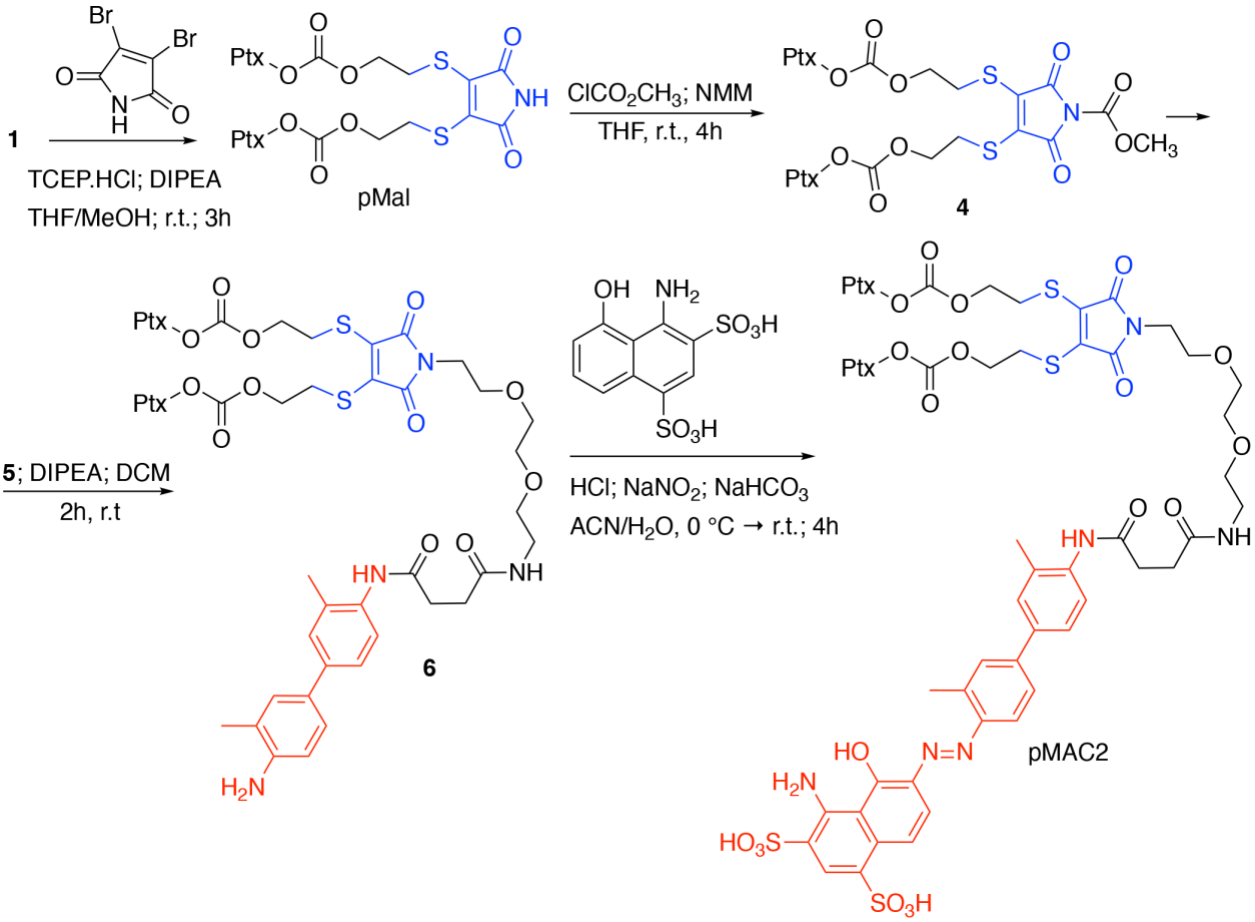

Scheme 2. Synthetic route to pMAC2.

Conjugates pMAC1 and pMAC2 are characterized by the presence of 2 molecules of Ptx connected through bioresponsive linkers to the HSA-targeting moiety tEB and are reported here for the first time. It is worth noticing that, unlike what previously reported on other drug-tEB conjugates in which tEB is coupled with the target molecule as the final reaction step,[30,31] the procedure herein developed foresees the diazotization reaction as the last synthetic step. Indeed, in our hand, the direct coupling between tEB and any precursor's prodrug afforded poor yields and required tedious and unsuccessful purification procedures. Conversely, the mild conditions of the diazotization reaction allow to easily access the desired compounds. In principle, this unprecedent synthetic procedure can drive the simple and straightforward tEB functionalization of several

active ingredients with the aim of improving their blood circulation time and preferential tumor accumulation by binding with endogenous HSA.

By following a similar synthetic strategy, the bioresponsive and HSA-binding analogue of Nlg, i.e., nMAC (Scheme 3), was successfully synthesized for the first time starting from commercially available Nlg. Compound **7** was obtained in 52% yield by reacting Nlg with triphosgene and 2-hydroxyethyldisulfide. Activation with *p*-nitrophenyl chloroformate afforded derivative **8** in 60% yield that upon reaction with compound **5** (Scheme S3) provided the precursor **9** in 32% yield. The last diazotization step followed by dialysis purification allowed to isolate the nMAC conjugate in 70% yield.

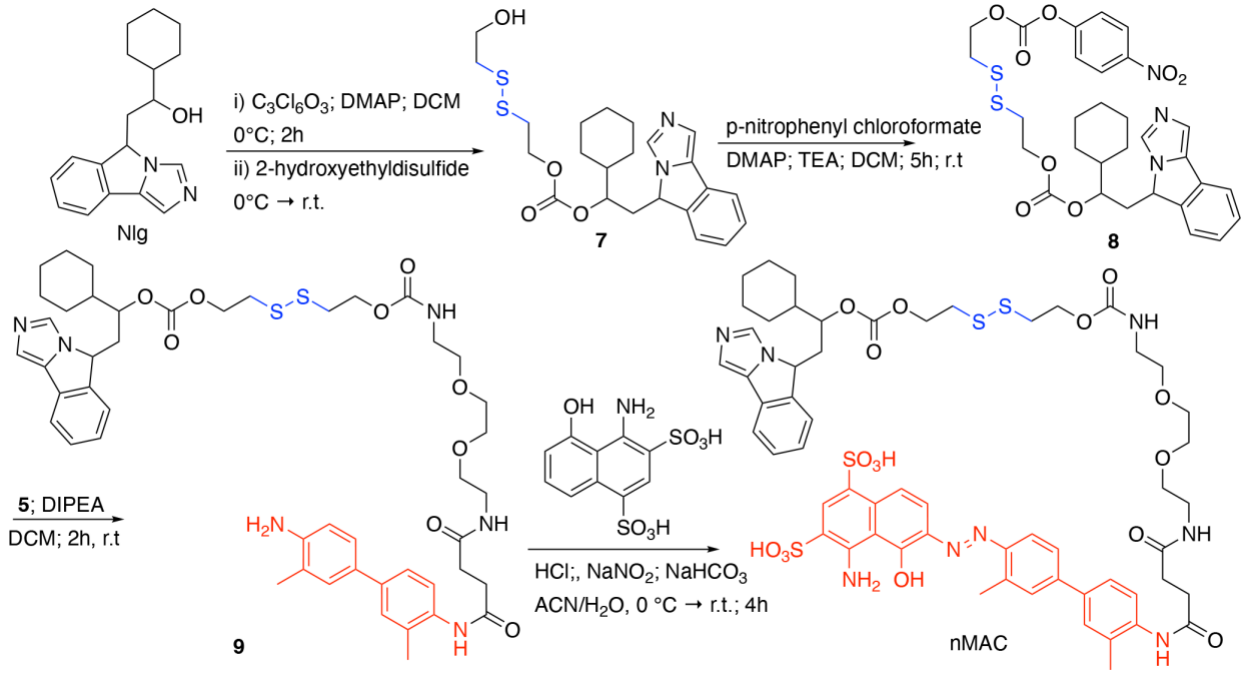

Scheme 3. Synthetic route to nMAC.

3.2. MACs characterization: HSA binding affinity of Ptx-based MACs

A SPR analysis was performed to confirm that the chemical modifications on tEB (Scheme S1) did not compromise the ability to bind HSA. Within the same investigation the binding affinity of pMAC1, pMAC2 and nMAC to HSA with reference to tEB was assessed. To this aim, a HSA-

functionalized sensor chip was prepared by immunocapturing HSA onto a CM5 sensor chip previously functionalized with an anti-HSA antibody. Non-specific interactions of analytes with the surface antibody were zeroed by functionalizing in parallel the reference flow cell with the same antibody. Due to the expected low dissociation rates of Evan blue-HSA complexes, a single-cycle kinetics was used for the determination of the affinity constants. Interaction between tEB and HSA resulted in a K_D value of 20.7 ± 1.5 μM. Investigations on MAC derivatives confirmed that structural modifications did not hamper their ability to bind HSA. Conversely, all derivatives showed a slightly higher affinity for HSA, when compared to tEB, although in the same order of magnitude. This lets us speculate that the higher structural complexity of MACs further contributes to complex stabilization. K_D values for tEB and MACs are summarized in Table 1.

Table 1. HSA binding affinities of tEB and Ptx-based MACs, as determined by SPR analysis. Results are averaged over two independent experiments.

Compound	**K_D (μM)**
tEB	20.7 ± 1.5
pMAC1	14.6 ± 0.1
pMAC2	8.1 ± 1.1
nMAC	8.5 ± 0.1

3.3. MACs characterization: stability of MACs in solution

The sensitivity of MACs towards the redox potential of the surrounding environment was evaluated by means of stability studies in solution. MACs (pMAC1, pMAC2, nMAC) and the main precursor of Ptx-based MACs (pMal) were exposed to increasing concentrations (0 to 1000-

fold molar excess) of dithiothreitol (DTT), incubated for 3 h in the presence or absence of equimolar quantities of HSA and analyzed by HPLC-UV.

A protective effect of HSA against reduction by DTT was observed for all prodrugs, albeit to different extents (Figure 2A). In particular, the stability of pMal and pMAC2 in strongly reducing conditions improved significantly in the presence of HSA, while pMAC1 and nMAC were less protected (Figure 2B): a possible explanation for this behavior in solution is given by the combined affinity of Ptx and tEB towards HSA. For pMal, the interaction with HSA is mainly driven by Ptx leading to a reduced exposure of the redox-sensitive dithiomaleimide moiety (lower release). On the other hand, MACs can interact with HSA also through the tEB moiety: however, the longer linker in the nMAC backbone leaves the disulphide bond too exposed to the environment, while the direct link between the dithiomaleimide ring and the tEB moiety may lead to a sub-optimal interaction of pMAC1 with HSA. In this framework, the PEG linker of pMAC2 seems to provide a balanced combination between HSA binding and redox sensitivity.

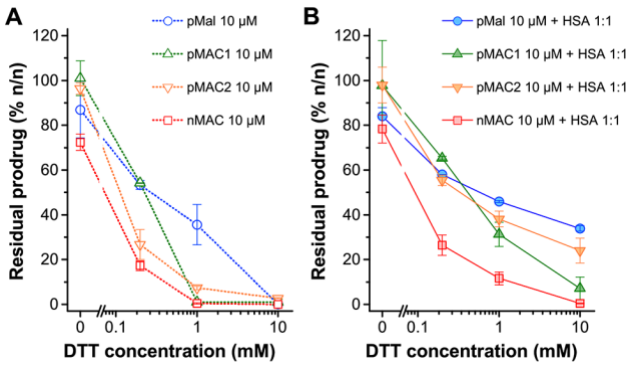

Figure 2. Stability of pMal and MACs (10 µM in PBS/EtOH 75:25 v/v) as a function of redox potential (DTT concentration), as determined by HPLC-UV analysis after 3 h incubation at 20 °C. **(A)** In the absence of HSA and **(B)** in the presence of HSA in equimolar ratio. Results are averaged over two independent experiments.

3.4. Preparation and characterization of NBs

We designed and generated different NBs including different combinations of MACs and bioresponsive dimeric prodrugs (pMal and NlgD), as well as single-component and dual-loaded "MAC-devoid" micelles, e.g., @pMal, @NlgD and @pMal-NlgD, respectively. NlgD and pMal were loaded into NBs to exploit their intrinsic ability to aid the stabilization of micelles [32] and to widen the versatility of nanosystems in terms of drug ratio, allowing to finely tune and optimize the concentration of both drugs inside the formulation and ultimately at the tumor site. HSA-binding NBs (Figure 3) were prepared by the nanoprecipitation method, [33] and several procedures and experimental conditions were tested to optimize NBs formation in terms of hydrodynamic diameter, polydispersity index (PDI) and stability in different media.

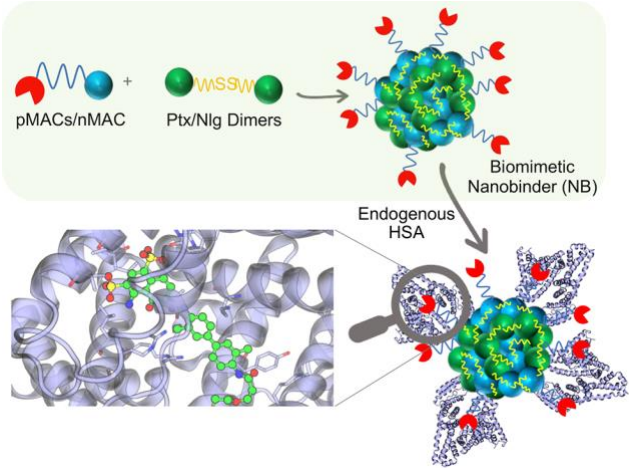

Figure 3 Schematic representation of biomimetic NB composition and mechanism of action.

The different physicochemical properties of prodrugs required tailored conditions for NBs preparation; therefore, four parameters were systematically investigated: the organic solvent for prodrug dissolution (DMF, DMSO or EtOH); the amount of water used for the nanoprecipitation; the order of addition of the water and organic phases; the purification method, i.e., dialysis, ultrafiltration (UF) or centrifugation. Ultimately, two different preparation procedures were

optimized for single-component micelles, e.g., @pMal and @NlgD, and multi components micelles, e.g., @pMal-NlgD, NBs and fluorescent NBs, respectively (see § 2.4).

The preparation of MAC-devoid micelles resulted in the formation of stable particles with satisfactory size (120–150 nm) and polydispersity indexes (Table S3),[34] as observed by dynamic light scattering (DLS) measurements. Regardless of the preparation procedure and drug contents, multi-component NBs containing pMAC1 were significantly less stable than those containing pMAC2, resulting either in precipitation over time or in highly polydisperse micelles (Tables 2 and S4). These results, combined with those on prodrugs' stability (Figure 2) and HSA binding affinity (Table 1), suggest that the short PEG chain in the pMAC2 structure might also aid NB stabilization and interaction with the protein, prompting us to identify pMAC2 as the most promising prodrug for further NB development.

Table 2. Ratiometric design and DLS characterization of selected NB formulations.

Entry	Sample	Nlg/Ptx ratio (n/n)	MAC loading (n/n)	Diameter (nm)	PDI
1	**pMAC1**@NB1	0.49	67%	232.6 ± 15.1	0.331 ± 0.047
2	**pMAC1**@NB2	0.33	75%	87.0 ± 5.6	0.489 ± 0.059
3	**pMAC1**@NB3	0.82	55%	50.4 ± 7.1	0.365 ± 0.076
4	**pMAC1**@NB4	0.47	80%	65.0 ± 11.3	0.479 ± 0.107
5	**pMAC2**@NB1	0.63	61%	241.8 ± 9.6	0.278 ± 0.089
6	**pMAC2**@NB2 **(NB@2)**	1.54	39%	87.2 ± 2.2	0.142 ± 0.002
7	**pMAC2**@NB3	4.13	37%	75.0 ± 4.4	0.184 ± 0.047
8	**pMAC2**@NB4	4.76	26%	49.3 ± 2.7	0.365 ± 0.028

9	**pMAC2**@NB5 **(NB@5)**	3.51	50%	92.1 ± 1.3	0.133 ± 0.001

An optimization study was then carried out to identify the most favorable conditions to produce pMAC2-based NBs with different prodrug ratios (Table S4), resulting in different Nlg/Ptx ratios (0.6–4.8, n/n), MAC loading ratios (a proxy for tEB functionalization; 39–64%, n/n) and hydrodynamic diameters (49–242 nm). As a result, two formulations, namely NB@2 and NB@5 (entries 6 and 9, Table 2), were selected as the most promising based on their composition, polydispersity, reproducibility, and stability over time. NB@2 and NB@5 have similar hydrodynamic diameters and MAC loading ratios, while the Nlg/Ptx ratio is more than double for NB@5 compared to NB@2. Indeed, preliminary *in vitro* cytotoxicity and IDO1 inhibition experiments on MDA-MB-268 TNBC cells showed that, despite having similar cells growth inhibition activity (Figure 4A), NB@5 were significantly more effective in reducing the IDO1 enzymatic activity (Figure 4B); therefore, NB@5 were selected for in depth physical-chemical and *in vitro* characterization.

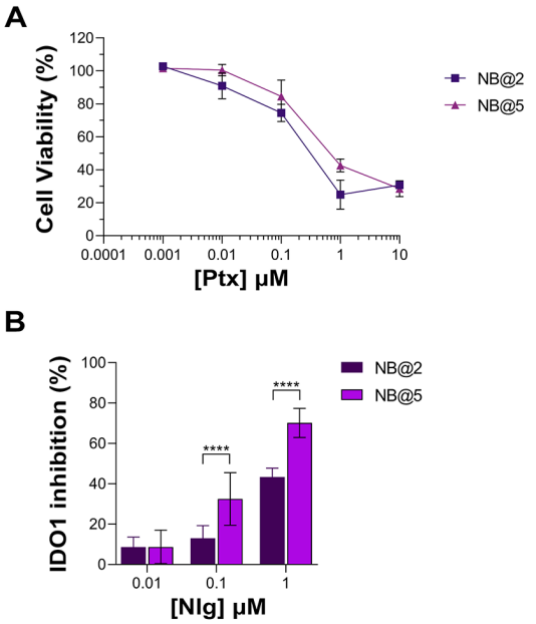

Figure 4 (A) Evaluation of cytotoxicity of NB@2 and NB@5 on MDA-MB-468 cells after 48 h of exposure. **(B)** Evaluation of IDO1 inhibition rate (%) in MDA-MB-468 cells after 24 h of exposure to NBs. Data are expressed as mean ± SD of at least two independent experiments carried out in triplicate. Data were analyzed using the 2-way ANOVA test, and Bonferroni's multiple comparison as a post-test. Results were statistically significant for p-values < 0.05 (****p-values< 0.0001).

NB@5 are tri-components micelles composed of pMAC2, nMAC and NlgD to a final Nlg/Ptx molar ratio of 3.5 and a 50% MAC loading. DLS stability studies were performed in PBS pH 7.4 (37 °C, 24 h) with or without HSA (35 mg/mL) and FBS (10%, v/v): NB@5 showed good stability profiles both in terms of hydrodynamic diameters and polydispersity (Figure 5A). Transmission electron microscopy (TEM) studies allowed to assess the morphology of NB@5. In the absence of HSA, NB@5 show a spherical shape with average dry diameters of about 50 nm (Figure 5B). Upon incubation with excess HSA (10:1, m/m), an irregular protein corona was observed around NB@5, supporting the hypothesis of an interaction between NBs and the protein mediated by tEB

(Figure 5C). Indeed, treatment with HSA in the same conditions did not lead to the formation of a protein corona around MAC-devoid micelles @pMal-NlgD (Figure S22), further confirming the key role played by tEB in promoting the binding of HSA to NBs.

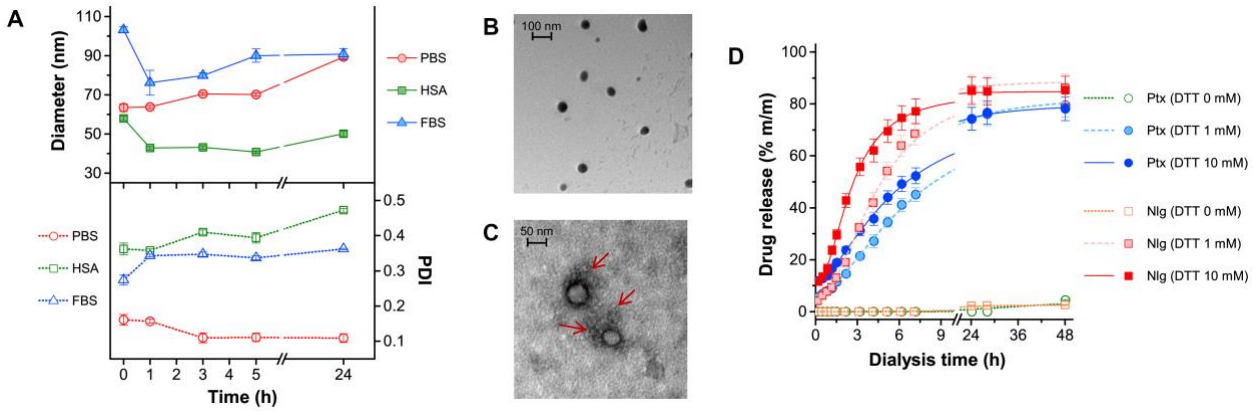

Figure 5 (A) NB@5 stability in PBS, PBS + HSA and PBS + FBS at 37 °C, as evaluated by DLS analysis. **(B)** TEM analysis of NB@5 (scale bar: 100 nm). **(C)** TEM analysis of NB@5 pre-incubated with HSA (10:1, m/m; scale bar: 50 nm). **(D)** Release profiles of Ptx and Nlg from NB@5 in different redox conditions, as determined by equilibrium dialysis and HPLC–UV analysis.

The kinetics of Ptx and Nlg release from NB@5 was evaluated by HPLC–UV analysis (Figure 5D) after equilibrium dialysis (37 °C, 48 h) in PBS/EtOH 75:25 v/v with increasing concentrations of DTT (0–10 mM). As expected, the release of drugs in non-reducing conditions is negligible, while the kinetic curves in reducing conditions show that both Ptx and Nlg are released faster as the concentration of DTT increases, further supporting the redox-sensitive mechanism of prodrug conversion.

3.5. In vitro activity of bioresponsive and HSA-binding building blocks

The capability of bioresponsive pMAC2 of inducing cytotoxicity and IDO1 inhibition was assessed *in vitro* in MDA-MB-468 TNBC cells. Upon incubation with increasing concentration of

pMal, pMAC2 or Ptx for 48 h, cell viability was assessed by the MTS assay at the end of incubation time. Cell viability reduction was concentration-dependent for all Ptx derivatives up to 1 μM, while above this concentration a plateau was reached (35-20 % cell viability) (Figure 6A). As expected, the IC_{50} value of pMAC2 (0.690 ± 0.005 μM) was significantly higher as those of pMal (0.050 ± 0.012 μM) and Ptx (0.034 ± 0.001 μM). The reduced cytotoxic effect of pMAC2 compared to pMal highlights the crucial role of protein binding, mediated by the tEB moiety, in controlling Ptx release.

The IDO1 inhibitory capacity of Nlg and Nlg prodrugs, i.e., NlgD and nMAC, in MDA-MB-468 cells stimulated with IFN-γ to further over-express the enzyme, was measured indirectly by monitoring the decrease of Kyn release in the medium after 24 h of cell incubation. The percentage of IDO1 inhibition was almost complete when 10 μM Nlg and Nlg prodrugs were administered to cells (Figure 6B) and persisted almost unaltered for the following 24 h (data not shown). At 1 μM Nlg concentration, the inhibitory activity was significantly higher for free Nlg (ca. 80%), followed by NlgD (ca. 60%) and nMAC (ca. 40%) after 24 h, while being comparable at 10 μM Nlg equivalent.

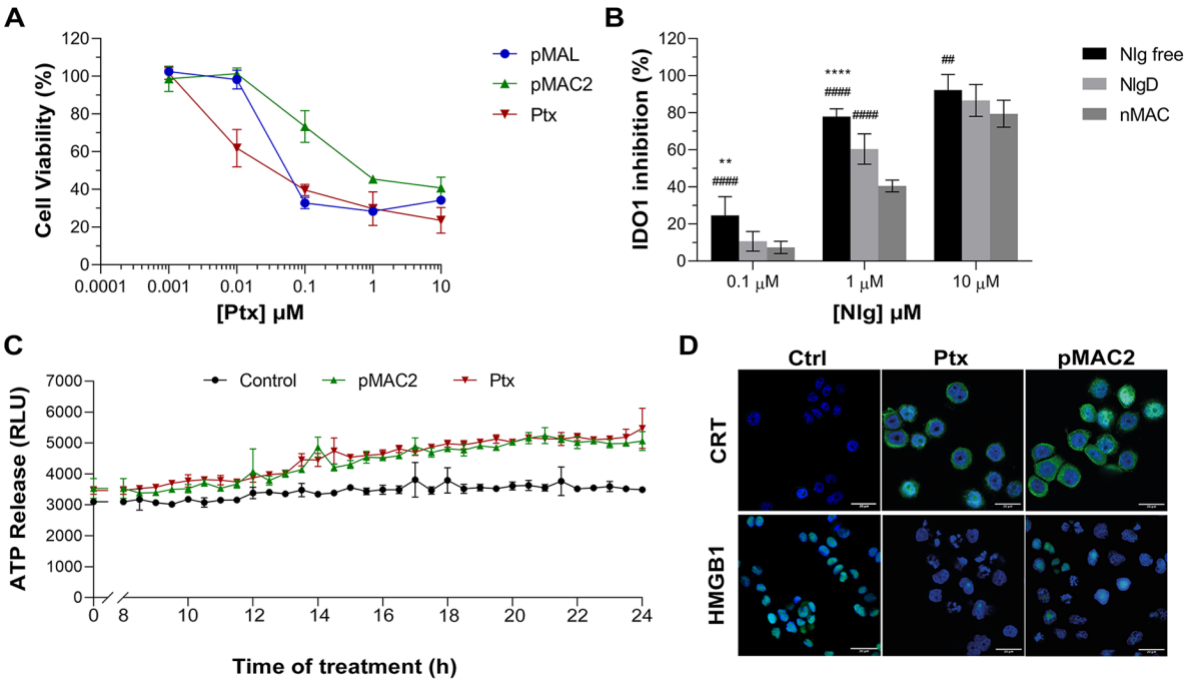

Figure 6 (A) Viability curves of MDA-MB-468 cells exposed to increasing concentrations of Ptx and Ptx bioresponsive conjugates measured by MTS tests after 48 h of incubation. **(B)** IDO1 inhibition rate (%) in MDA-MB-468 cells incubated with the compounds for 24 h. **(C)** ATP release in the cell culture medium of cells exposed to drugs at Ptx concentration 1µM for 24 h. **(D)** Immunofluorescence images of cells incubated with the compounds at Ptx concentration 1µM for 12 h and stained with antibody against CRT and HMGB1- FITC conjugated (green) and with Hoechst 33342 (blue) for nuclei recognition. Scale bar: 20 µm. Data are expressed as mean ± SD of at least 2 independent experiments carried out in triplicate and statistical analysis has been generated using the 2-way ANOVA test, and Bonferroni's multiple comparison as a post-test. Results were considered statistically significant at p-values < 0.05 (* p-values < 0.05, ** p-values < 0.01, *** p-values < 0.001 and **** p-values < 0.0001). Data compared to NlgD are reported as *, while data compared to nMAC are indicated with #.

One important aspect of our rationale is boosting IDO1 inhibition and Ptx-induced cytostatic effect with an early stimulation of ICD orchestrated by pMAC2. Therefore, we assessed the occurrence of the three principal ICD hallmarks, *i.e.,* ATP release, calreticulin (CRT) exposure on extracellular plasma membrane, and high-mobility group box 1 (HMGB1) translocation/release,[35] in MDA-MB-468 cells exposed to Ptx and pMAC2. The kinetic of ATP release in the cell culture medium of cells exposed to 1.0 μM Ptx equivalent determined a not significantly different ATP release when free Ptx and pMAC2 prodrug were administered to cells (Figure 6C). Immunofluorescence and confocal microscopy were used to investigate CRT exposure and HMGB1 translocation/release in cells exposed for 12 h to 1 μM of Ptx equivalent either as free molecule or pMAC2. Control cells clearly showed green signals diffused throughout the cytoplasm and in the nuclei for CRT and HMGB1, respectively (Figure 6D). Cells exposure to 1 μM Ptx equivalent induced CRT membrane translocation and HMGB1 cytoplasmatic or extracellular release in most of the analyzed cells (Figure 6D) to a very similar extent for Ptx and pMAC2, as confirmed by signal quantification (Figure S23) Importantly, these analyses collectively confirm that our unprecedent bioresponsive conjugate pMAC2 can induce ICD in our TNBC model similarly to unmodified Ptx.

3.6. NB@5 in vitro cytotoxicity, ICD induction and IDO1 inhibition

The cytotoxic potential of NB@5 toward TNBC *in vitro* models was evaluated in MDA-MB-231 and MDA-MB-468 cancer cell lines, and in normal epithelial cells of the same derivation (MCF-10A line) to assess NB@5 untargeted toxicity as compared to MAC-devoid micelles, i.e., @pMal and @pMal-NlgD (Figure 7A-C). The viability curves and the corresponding IC_{50} values (Table 4) confirmed that NB@5 was the less toxic formulation against both cancer and healthy epithelial cells as compared to MAC-devoid micelles, which show similar viability reduction

trends and IC_{50} values. Indeed, neither free Nlg nor @NlgD are cytotoxic toward TNBC cells at the tested concentrations (not shown), thus explaining the identical IC_{50} values of @pMal and @pMal-NlgD in MDA-MB-468 (~ 0.02 µM) and MDA-MB-231 (~ 0.04 µM) cells. Importantly, the same trend was also observed in normal MCF-10A cells where NB@5 resulted the less toxic formulation with an IC_{50} value (0.286 µM) four to six times higher than MAC-devoid micelles (Figure 7C).

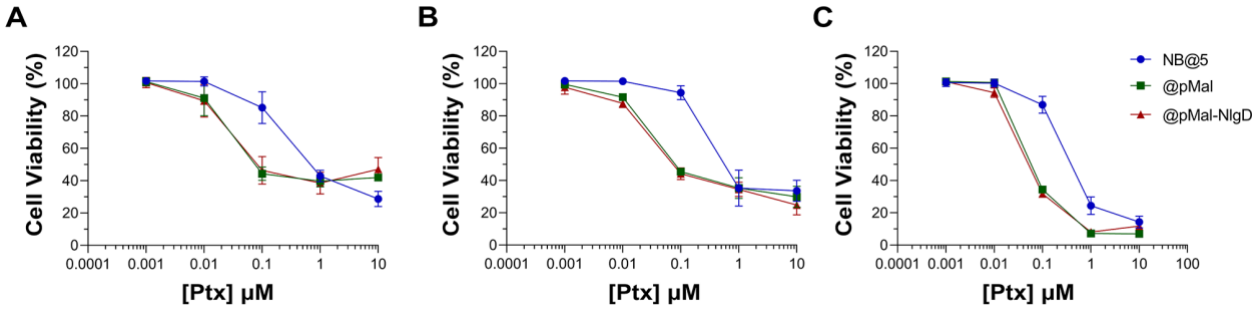

Figure 7 Evaluation of cytotoxicity in TNBC MDA-MB-468 **(A)** and MDA-MB-231 **(B)** and in normal breast MCF10A **(C)** cells exposed to drugs for 48 h.

Table 3 IC50 values of NB@5, @pMal and @pMal-NlgD in TNBC and normal epithelial breast cells.

Drugs	**Cell Lines**		
	MDA-MB-468(µM)	MDA-MB-231 (µM)	MCF10A (µM)
NB@5	0.298 ± 0.036	0.233 ± 0.065	0.286 ± 0.024
@pMal	0.023 ± 0.005	0.038 ± 0.005	0.070 ± 0.006
@pMal-NlgD	0.022 ± 0.006	0.037 ± 0.006	0.050 ± 0.003

We speculated that the reduced toxicity of NB@5 with respect to MAC-devoid micelles could be related to the presence of the tEB moiety on the NBs' surface and the consequent binding to serum albumins once diluted in cell culture medium (*e.g.,* basal medium supplemented with 10% FBS). Indeed, as earlier shown under reducing conditions, the release of Ptx from pMAC2 in solution is strongly reduced in the presence of HSA (Figure 2).

To further support this hypothesis, MDA-MB-468 cells were exposed to NB@5 nanoparticles that were pre-incubated with HSA or left untreated, in the presence of varying concentrations of DTT. At a Ptx equivalent concentration of 0.1 μM, only the pre-incubation of NBs with HSA led to higher cell viability (80%) under mild reducing conditions (10 μM DTT) Figure 8A. These findings further strengthen the role of the protein in modulating the release of Ptx under the physiological redox conditions commonly found in healthy tissues. Conversely, under compromised redox conditions (10 mM DTT), the protective effect of HSA was unremarkable (Figure 8A).

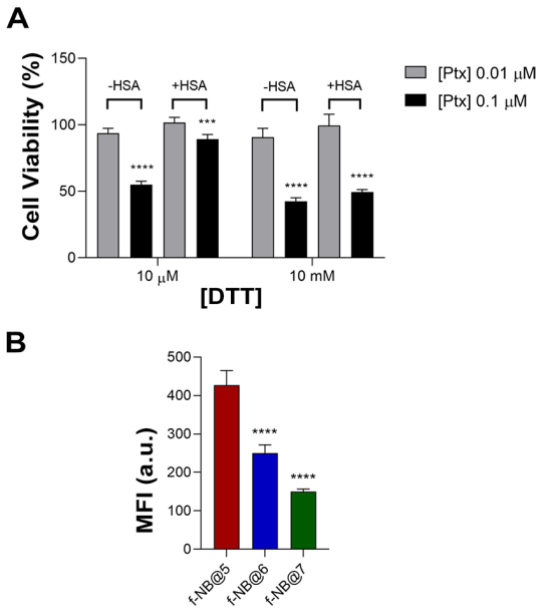

Figure 8 (A) Cell viability measured in MDA-MB-468 exposed for 48 h to NB@5 pre-incubated or not with HSA before cells treatment. Data are expressed as mean ± SD of at least two independent experiments carried out in triplicate; data were analyzed using the 2-way ANOVA test, and Bonferroni's multiple comparison as a post-test. Results were statistically significant for p-values < 0.05 (***p-values < 0.001, ****p-values < 0.0001). **(B)** Intracellular uptake measured by FACS in MDA-MB-468 cells treated with Nile Red-loaded NBs for 2 h. Data are expressed as mean ± SD of at least two independent experiments carried out in triplicate; data were analyzed using the one-way ANOVA test and Tukey's multiple comparison as post-test. Results were statistically significant at p-values < 0.05 (****p-values< 0.0001).

To gain more insight on the role of tEB on NBs protection and selectivity, we prepared additional fluorescently labelled NB formulations with similar Nlg/Ptx ratio as respect to NB@5 but with different MAC loading and incorporating the Nile Red (NR) fluorophore (f-NB@, Table S5). Our results indicate a pMAC2 loading-dependent intracellular uptake in MDA-MB-468 cells: the internalization rate of f-NB@6 and f-NB@7 (7% and 0% pMAC2 loading, respectively) was two

and three folds lower compared to f-NB@5 (14% pMAC2 loading) (Figure 8B). These results suggest that the interaction of NBs with serum proteins is mainly mediated by pMAC2. Indeed, despite the similar MAC loading of f-NB@5 and f-NB@7, the latter exhibits less cellular internalization, likely due to the lower capacity of nMAC to stabilize NB-HSA interaction through the tEB moiety. This observation is consistent with the limited protection provided by HSA to nMAC, as observed in stability studies, in comparison to pMAC2 (Figure 2).

Next, we evaluated whether NB@5 could successfully inhibit IDO1 enzymatic activity: our data confirmed a Nlg concentration-dependent Kyn conversion inhibition, which was almost complete when MDA-MB-468 cells were incubated for 24 h with 10 μM equivalent of Nlg incorporated into NBs (Figure 9A). Finally, we investigated the capability of NB@5 to drive ICD in TNBC cells. We measured a significant release of ATP in the extracellular media exclusively in MDA-MB-468 cells incubated with micelles containing 1 μM Ptx equivalent (Figure 9B-C), while in MDA-MB-231 cells the amount of ATP was not statistically different from control (not shown).

Finally, our data confirmed both CRT membrane translocation and HMGB1 nuclear release in MDA-MB-468 (Figure 9D, S24) and MDA-MB-231 cells (Figure S23) exposed to 1 μM Ptx equivalent for 12 h. The findings clearly demonstrate that NB@5 effectively trigger all the considered ICD hallmarks similarly to free Ptx, at least in MDA-MB-468 cells.

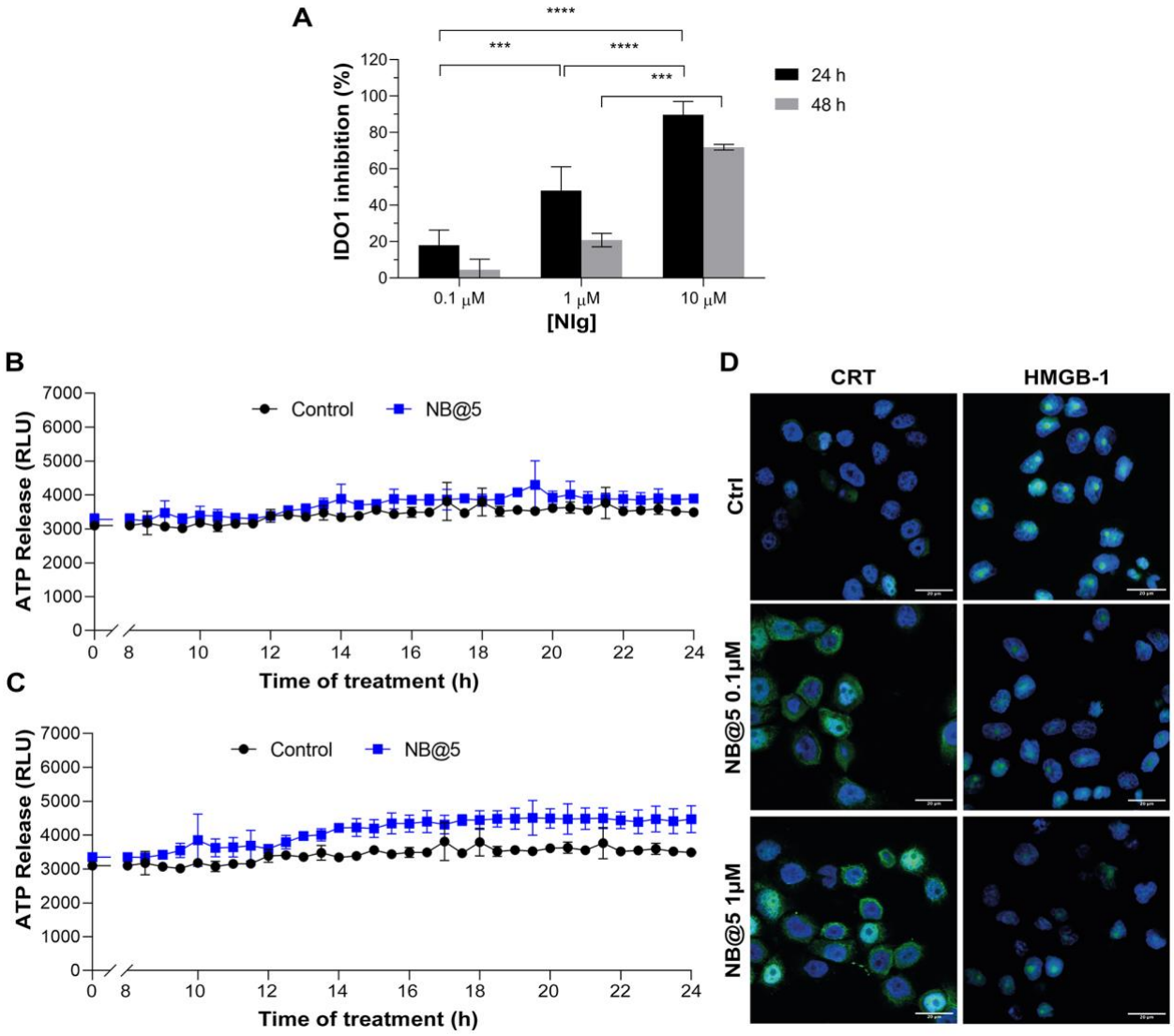

Figure 9 (A) IDO1 inhibition rate (%) in MDA-MB-468 cells incubated with different concentrations of Nlg incorporated into NB@5 for 24 h and 48 h; **(B-C)** ATP release in the cell culture medium of cells exposed to NB@5 (0.1 μM Ptx) **(B)** and NB@5 (1 μM Ptx) **(C)** for 24 h. **(D)** Immunofluorescence images of cells incubated with the compounds (1 μM Ptx) for 12 h and stained with antibody against CRT and HMGB1 FITC conjugated (green) and with Hoechst 33342 (blue) for nuclei recognition. Scale bar: 20μm. Data are expressed as mean ± SD of at least 2 independent experiments carried out in triplicate; statistical analysis has been generated using the 2-way ANOVA test, and Tukey's multiple comparison as a post-test. Results were considered

statistically significant at p-values < 0.05 (* p-values < 0.05, ** p-values < 0.01, *** p-values < 0.001 and **** p-values < 0.0001).

3.7. In vitro studies of NBs activity on TNBC cells spheroids

To preliminary evaluate the anticancer and immunomodulating activity of NB@5 in an *in vitro* model resembling more closely *in vivo* solid tumors, we measured cell viability reduction and IDO1 inhibition activity in MDA-MB-468 cell-derived three-dimensional spheroids. Therefore, 4-days old spheroids were incubated for 72 h with Ptx formulations before assessing viability reduction using the 3D Glo assay. As depicted in Figure 10A, the cytotoxicity trend was similar to that observed in 2D cancer cell models, showing that at low concentrations of Ptx, NB@5 and pMAC2 were significantly less toxic compared to Ptx and @pMal. However, no significant differences in viability reduction were observed at higher Ptx concentrations. As evident from the bright field images of treated spheroids (Figure 10B), all treatments caused alterations in the morphological structure of the spheroids, leading to a loss of their spherical shape in comparison to the control group. However, the volume reduction was not statistically different (not shown). IDO1 inhibition rate was measured in spheroids exposed to NB@5 and Nlg prodrugs for 48 h. Our results indicate that both NB@5 and Nlg prodrugs effectively reduce IDO1 enzymatic activity (around 50%), although to a lesser extent as respect to 2D models and with less evident dose-inhibition dependency (Figure 10C).

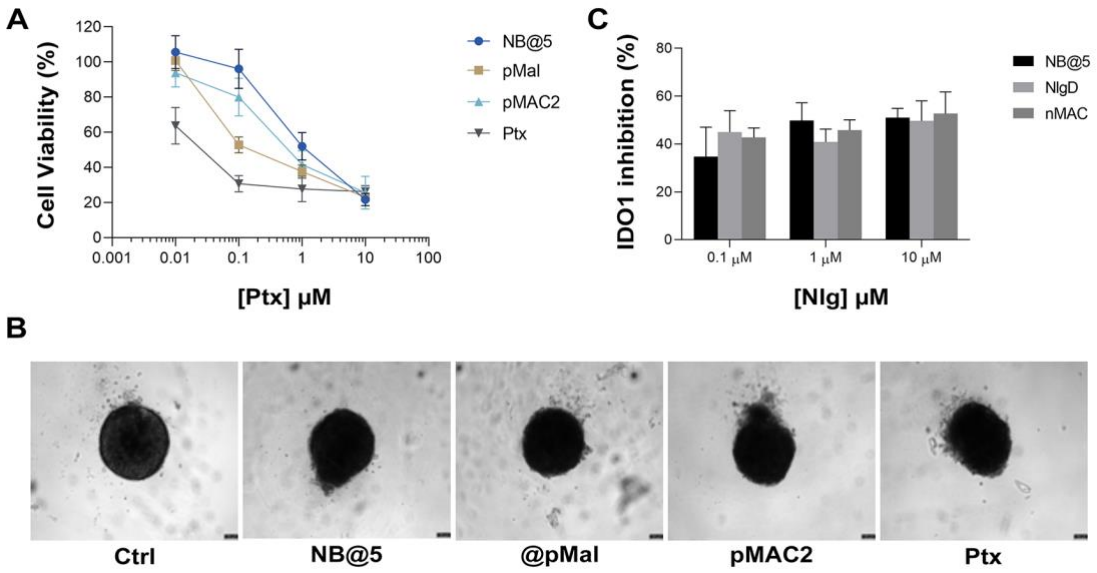

Figure 10 (A) Cytotoxicity measured in MDA-MB-468 spheroids treated for 72 h with NB@5 and reference compounds at increasing Ptx concentration and assessed with the CellTiter-Glo® 3D assay. **(B)** Bright field images of treated spheroids at Ptx concentration corresponding to 1µM. Scale bar: 100 µm. **(C)** IDO1 inhibition (%) calculated measuring Kyn content in the cell culture medium of cells exposed to drugs for 48 h.

4. CONCLUSIONS

Targeting IDO1 in combination with ICD-inducing chemotherapeutic agents represents a promising therapeutic opportunity to enhance both the activation and maintenance of tumor-specific T-cell immune response within the tumor microenvironment. However, important considerations should be drawn when considering combination therapy, such as uneven drugs accumulation at the target tissue and premature drugs release. In this view, the use of inactive prodrugs with their concomitant encapsulation into suitably designed nanocarriers could provide unique advantages over the administration of free drugs, such as protection against degradation, prolonged circulation time, improved pharmacokinetic, sustained drug release, and ability to deliver insoluble drugs.

Our study reports the unprecedented synthesis of HSA-binding and biomimetic prodrugs, forming stable and reproducible carrier-free nanobinders with tunable drugs ratios and serum albumin binding functionalization.

The data obtained from our research strongly support the hypothesis that NB@5 effectively bind with HSA, demonstrating its protective role in the controlled release of drugs *in vitro* and suggesting that our nanobinders can exploit the protein as an endogenous shuttle for targeted delivery to tumor site *in vivo*. Furthermore, our study successfully demonstrates that the drugs encapsulated in the nanobinders are preferentially released under the altered redox conditions typically found in the tumor microenvironment, and are capable of inducing cell death, drive ICD and inhibit IDO1. Considering the limitations of *in vitro* settings, especially for the evaluation of complex molecular pathways involving the whole tumor microenvironment, a preclinical *in vivo* assessment of our NBs is in the pipeline to leap the system closer to clinical translation.

AUTHOR INFORMATION

Corresponding Author

*Correspondence to:

Greta Varchi, Ph.D., Institute of Organic Synthesis and Photoreactivity – Italian National Research Council Via Piero Gobetti 101, 40129, Bologna, Italy. Email: greta.varchi@isof.cnr.it.

Francesca Moret, Ph.D., Department of Biology (DiBio), University of Padova, Via U. Bassi 58/B, 35100 Padova, Italy. Email: francesca.moret@unipd.it.

Author Contributions

The manuscript was written through contributions of all authors. All authors have given approval to the final version of the manuscript.

‡These authors contributed equally.

Funding Sources

This research was financially supported by the Worldwide Cancer Research, grant number 21-0028 to G.V., as well as by the National Recovery and Resilience Plan (NRRP), Mission 04 Component 2 Investment 1.5 – NextGenerationEU, Call for tender n. 3277 (30/12/2021) Award Number: 0001052 (23/06/2022)

ACKNOWLEDGMENT

This research was financially supported by the Worldwide Cancer Research, grant number 21-0028 to G.V., as well as by the National Recovery and Resilience Plan (NRRP), Mission 04 Component 2 Investment 1.5 – NextGenerationEU, Call for tender n. 3277 (30/12/2021) Award Number: 0001052 (23/06/2022)

ABBREVIATIONS

CAN, acetonitrile; AcOH, acetic acid; AHR, aryl hydrocarbon receptor; APC, antigen-presenting receptor; ATP, adenosine 5′-triphosphate; CD_3OD, methanol-d4; $CDCl_3$, chloroform-d; cHex, cyclohexane; CO_2, carbon dioxide; CRT, calreticulin; D_2O, deuterium oxide; DAMP, damage-associated molecular pattern; DCM, dichloromethane; DIPEA, N,N-diisopropylethylamine; DLS, dynamic light scattering; DMAP, 4-dimethylaminopyridine; DMEM, Dulbecco's modified Eagle medium; DMF, N,N-dimethylformamide; DMSO, dimethyl sulfoxide; DMSO-d_6, dimethyl sulfoxide-d_6; DTT, dithiothreitol; EGF, epidermal growth factor;

Et_2O, diethyl ether; EtOAc, ethyl acetate; EtOH, ethanol; FBS, foetal bovine serum; Gly, glycine; HCl, hydrochloric acid; HMGB1, high-mobility group box 1 protein; HPLC, high-performance liquid chromatography; HSA, human serum albumin; ICD, immunogenic cell death; IDO1, indoleamine-2,3-dioxygenase enzyme; IFN-γ, interferon-γ; K_D, binding dissociation constant; Kyn, L-kynurenine; MeOH, methanol; $MgSO_4$, magnesium sulfate; mTORC1, mammalian target of rapamycin complex 1; MTS, 3-(4,5-dimethylthiazol-2-yl)-5-(3-carboxymethoxyphenyl)-2-(4-sulfophenyl)-2H-tetrazolium; MWCO, molecular weight cut-off; Na_2SO_4, sodium sulfate; $NaHCO_3$, sodium bicarbonate; $NaNO_2$, sodium nitrite; NaOH; sodium hydroxide; NB, nanobinder; NH_4Cl, ammonium chloride; NH_4OAc, ammonium acetate; Nlg, NLG919; NlgD, NLG919 dimer with disulfide linker; nMAC, NLG919 modular affinity conjugate; NMM, N-methylmorpholine; NMR, nuclear magnetic resonance; PBS, phosphate buffered saline; PDA, photodiode array; pMAC1, paclitaxel modular affinity conjugate 1; pMAC2, paclitaxel modular affinity conjugate 2; pMal, paclitaxel dimer with maleimide linker; Ptx, paclitaxel; PyBOP, (benzotriazol-1-yloxy)tripyrrolidinophosphonium hexafluorophosphate; RES, reticuloendothelial system; TCEP, tris(2-carboxyethyl)phosphine; TEA, triethylamine; tEB, truncated Evans Blue; TEM, transmission electron microscopy; TFA, trifluoroacetic acid; THF, tetrahydrofuran; TIPS, triisopropylsilane; TLC, thin-layer chromatography; TME, tumor microenvironment; TNBC, triple-negative breast cancer; Trp, L-tryptophan.

REFERENCES

(1) Yin, L.; Duan, J.-J.; Bian, X.-W.; Yu, S. Triple-Negative Breast Cancer Molecular Subtyping and Treatment Progress. *Breast Cancer Research* **2020**, *22* (1), 61. https://doi.org/10.1186/s13058-020-01296-5.

(2) Bianchini, G.; Angelis, C. D.; Licata, L.; Gianni, L. Treatment Landscape of Triple-Negative Breast Cancer – Expanded Options, Evolving Needs. *Nature Reviews Clinical Oncology* **2022**, *19* (2), 91–113. https://doi.org/10.1038/s41571-021-00565-2.

(3) Guan, J.; Wu, Y.; Liu, X.; Wang, H.; Ye, N.; Li, Z.; Xiao, C.; Zhang, Z.; Li, Z.; Yang, X. A Novel Prodrug and Its Nanoformulation Suppress Cancer Stem Cells by Inducing Immunogenic Cell Death and Inhibiting Indoleamine 2, 3-Dioxygenase. *Biomaterials* **2021**, *279* (September), 121180. https://doi.org/10.1016/j.biomaterials.2021.121180.

(4) Loizides, S.; Constantinidou, A. Triple Negative Breast Cancer: Immunogenicity, Tumor Microenvironment, and Immunotherapy. *Front Genet* **2022**, *13*, 1095839. https://doi.org/10.3389/fgene.2022.1095839.

(5) Marra, A.; Viale, G.; Curigliano, G. Recent Advances in Triple Negative Breast Cancer: The Immunotherapy Era. *BMC Medicine* **2019**, *17* (1), 90. https://doi.org/10.1186/s12916-019-1326-5.

(6) Loi, S.; Drubay, D.; Adams, S.; Pruneri, G.; Francis, P. A.; Lacroix-Triki, M.; Joensuu, H.; Dieci, M. V.; Badve, S.; Demaria, S.; Gray, R.; Munzone, E.; Lemonnier, J.; Sotiriou, C.; Piccart, M. J.; Kellokumpu-Lehtinen, P.-L.; Vingiani, A.; Gray, K.; Andre, F.; Denkert, C.; Salgado, R.; Michiels, S. Tumor-Infiltrating Lymphocytes and Prognosis: A Pooled Individual Patient Analysis of Early-Stage Triple-Negative Breast Cancers. *JCO* **2019**, *37* (7), 559–569. https://doi.org/10.1200/JCO.18.01010.

(7) Alkhayyal, N.; Elemam, N. M.; Hussein, A.; Magdub, S.; Jundi, M.; Maghazachi, A. A.; Talaat, I. M.; Bendardaf, R. Expression of Immune Checkpoints (PD-L1 and IDO) and Tumour-

Infiltrating Lymphocytes in Breast Cancer. *Heliyon* **2022**, *8* (9), e10482. https://doi.org/10.1016/j.heliyon.2022.e10482.

(8) Keenan, T. E.; Tolaney, S. M. Role of Immunotherapy in Triple-Negative Breast Cancer. *Journal of the National Comprehensive Cancer Network* **2020**, *18* (4), 479–489. https://doi.org/10.6004/jnccn.2020.7554.

(9) Beckers, R. K.; Selinger, C. I.; Vilain, R.; Madore, J.; Wilmott, J. S.; Harvey, K.; Holliday, A.; Cooper, C. L.; Robbins, E.; Gillett, D.; Kennedy, C. W.; Gluch, L.; Carmalt, H.; Mak, C.; Warrier, S.; Gee, H. E.; Chan, C.; McLean, A.; Walker, E.; McNeil, C. M.; Beith, J. M.; Swarbrick, A.; Scolyer, R. A.; O'Toole, S. A. Programmed Death Ligand 1 Expression in Triple-Negative Breast Cancer Is Associated with Tumour-Infiltrating Lymphocytes and Improved Outcome. *Histopathology* **2016**, *69* (1), 25–34. https://doi.org/10.1111/his.12904.

(10) Li, P.; Wu, R.; Li, K.; Yuan, W.; Zeng, C.; Zhang, Y.; Wang, X.; Zhu, X.; Zhou, J.; Li, P.; Gao, Y. IDO Inhibition Facilitates Antitumor Immunity of Vγ9Vδ2 T Cells in Triple-Negative Breast Cancer. *Frontiers in Oncology* **2021**, *11* (July), 1–14. https://doi.org/10.3389/fonc.2021.679517.

(11) Zhang, J.; Huang, D.; Saw, P. E.; Song, E. Turning Cold Tumors Hot: From Molecular Mechanisms to Clinical Applications. *Trends in Immunology* **2022**, *43* (7), 523–545. https://doi.org/10.1016/j.it.2022.04.010.

(12) Nel, A. E.; Mei, K. C.; Liao, Y. P.; Liu, X. Multifunctional Lipid Bilayer Nanocarriers for Cancer Immunotherapy in Heterogeneous Tumor Microenvironments, Combining Immunogenic Cell Death Stimuli with Immune Modulatory Drugs. *ACS Nano* **2022**, *16* (4), 5184–5232. https://doi.org/10.1021/acsnano.2c01252.

(13) Ye, Z.; Yue, L.; Shi, J.; Shao, M.; Wu, T. Role of IDO and TDO in Cancers and Related Diseases and the Therapeutic Implications. *Journal of Cancer* **2019**, *10* (12), 2771–2782. https://doi.org/10.7150/jca.31727.

(14) Nguyen, N. T.; Kimura, A.; Nakahama, T.; Chinen, I.; Masuda, K.; Nohara, K.; Fujii-Kuriyama, Y.; Kishimoto, T. Aryl Hydrocarbon Receptor Negatively Regulates Dendritic Cell Immunogenicity via a Kynurenine-Dependent Mechanism. *Proceedings of the National Academy of Sciences* **2010**, *107* (46), 19961–19966. https://doi.org/10.1073/pnas.1014465107.

(15) Girithar, H.-N.; Staats Pires, A.; Ahn, S. B.; Guillemin, G. J.; Gluch, L.; Heng, B. Involvement of the Kynurenine Pathway in Breast Cancer: Updates on Clinical Research and Trials. *Br J Cancer* **2023**, *129* (2), 185–203. https://doi.org/10.1038/s41416-023-02245-7.

(16) Zhai, L.; Ladomersky, E.; Lenzen, A.; Nguyen, B.; Patel, R.; Lauing, K. L.; Wu, M.; Wainwright, D. A. IDO1 in Cancer: A Gemini of Immune Checkpoints. *Cellular and Molecular Immunology* **2018**, *15* (5), 447–457. https://doi.org/10.1038/cmi.2017.143.

(17) Gao, J.; Deng, F.; Jia, W. Inhibition of Indoleamine 2,3-Dioxygenase Enhances the Therapeutic Efficacy of Immunogenic Chemotherapeutics in Breast Cancer. *Journal of Breast Cancer* **2019**, *22* (2), 196–209. https://doi.org/10.4048/jbc.2019.22.e23.

(18) Vanmeerbeek, I.; Sprooten, J.; De Ruysscher, D.; Tejpar, S.; Vandenberghe, P.; Fucikova, J.; Spisek, R.; Zitvogel, L.; Kroemer, G.; Galluzzi, L.; Garg, A. D. Trial Watch: Chemotherapy-Induced Immunogenic Cell Death in Immuno-Oncology. *OncoImmunology* **2020**, *9* (1), 1–23. https://doi.org/10.1080/2162402X.2019.1703449.

(19) Kroemer, G.; Galassi, C.; Zitvogel, L.; Galluzzi, L. Immunogenic Cell Stress and Death. *Nature immunology* **2022**, *23* (4), 487–500. https://doi.org/10.1038/S41590-022-01132-2.

(20) Bonaventura, P.; Shekarian, T.; Alcazer, V.; Valladeau-Guilemond, J.; Valsesia-Wittmann, S.; Amigorena, S.; Caux, C.; Depil, S. Cold Tumors: A Therapeutic Challenge for Immunotherapy. *Frontiers in Immunology* **2019**, *10* (FEB). https://doi.org/10.3389/fimmu.2019.00168.

(21) Fu, S.; Li, G.; Zang, W.; Zhou, X.; Shi, K.; Zhai, Y. Pure Drug Nano-Assemblies: A Facile Carrier-Free Nanoplatform for Efficient Cancer Therapy. *Acta pharmaceutica Sinica. B* **2022**, *12* (1), 92–106. https://doi.org/10.1016/J.APSB.2021.08.012.

(22) Zhang, Y.; Guo, Z.; Cao, Z.; Zhou, W.; Zhang, Y.; Chen, Q.; Lu, Y.; Chen, X.; Guo, Q.; Li, C.; Liang, D.; Sun, T.; Jiang, C. Endogenous Albumin-Mediated Delivery of Redox-Responsive Paclitaxel-Loaded Micelles for Targeted Cancer Therapy. *Biomaterials* **2018**, *183*, 243–257. https://doi.org/10.1016/j.biomaterials.2018.06.002.

(23) Hoogenboezem, E. N.; Duvall, C. L. Harnessing Albumin as a Carrier for Cancer Therapies. *Advanced drug delivery reviews* **2018**, *130* (1), 73–89. https://doi.org/10.1016/j.addr.2018.07.011.

(24) Rapozzi, V.; Moret, F.; Menilli, L.; Guerrini, A.; Tedesco, D.; Naldi, M.; Bartolini, M.; Gani, M.; Zorzet, S.; Columbaro, M.; Milani, C.; Martini, C.; Ferroni, C.; Varchi, G. HSA-Binding Prodrugs-Based Nanoparticles Endowed with Chemo and Photo-Toxicity against Breast Cancer. *Cancers* **2022**, *14* (4), 877. https://doi.org/10.3390/cancers14040877.

(25) Zhang, F.; Zhu, G.; Jacobson, O.; Liu, Y.; Chen, K.; Yu, G.; Ni, Q.; Fan, J.; Yang, Z.; Xu, F.; Fu, X.; Wang, Z.; Ma, Y.; Niu, G.; Zhao, X.; Chen, X. Transformative Nanomedicine of an

Amphiphilic Camptothecin Prodrug for Long Circulation and High Tumor Uptake in Cancer Therapy. *ACS Nano* **2017**, *11* (9), 8838–8848. https://doi.org/10.1021/acsnano.7b03003.

(26) Fan, J.; Gilmartin, K.; Octaviano, S.; Villar, F.; Remache, B.; Regan, J. Using Human Serum Albumin Binding Affinities as a Proactive Strategy to Affect the Pharmacodynamics and Pharmacokinetics of Preclinical Drug Candidates. *ACS Pharmacol. Transl. Sci.* **2022**, *5* (9), 803–810. https://doi.org/10.1021/acsptsci.2c00115.

(27) Chen, H.; Wang, G.; Lang, L.; Jacobson, O.; Kiesewetter, D. O.; Liu, Y.; Ma, Y.; Zhang, X.; Wu, H.; Zhu, L.; Niu, G.; Chen, X. Chemical Conjugation of Evans Blue Derivative: A Strategy to Develop Long-Acting Therapeutics through Albumin Binding. *Theranostics* **2016**, *6* (2), 243–253. https://doi.org/10.7150/thno.14322.

(28) Maciążek-Jurczyk, M.; Morak-Młodawska, B.; Jeleń, M.; Kopeć, W.; Szkudlarek, A.; Owczarzy, A.; Kulig, K.; Rogóż, W.; Pożycka, J. The Influence of Oxidative Stress on Serum Albumin Structure as a Carrier of Selected Diazaphenothiazine with Potential Anticancer Activity. *Pharmaceuticals* **2021**, *14* (3), 285. https://doi.org/10.3390/ph14030285.

(29) Castañeda, L.; Wright, Z. V. F.; Marculescu, C.; Tran, T. M.; Chudasama, V.; Maruani, A.; Hull, E. A.; Nunes, J. P. M.; Fitzmaurice, R. J.; Smith, M. E. B.; Jones, L. H.; Caddick, S.; Baker, J. R. A Mild Synthesis of N-Functionalised Bromomaleimides, Thiomaleimides and Bromopyridazinediones. *Tetrahedron Letters* **2013**, *54* (27), 3493–3495. https://doi.org/10.1016/j.tetlet.2013.04.088.

(30) Chen, H.; Jacobson, O.; Niu, G.; Weiss, I. D.; Kiesewetter, D. O.; Liu, Y.; Ma, Y.; Wu, H.; Chen, X. Novel "Add-on" Molecule Based on Evans Blue Confers Superior Pharmacokinetics and

Transforms Drugs to Theranostic Agents. *Journal of Nuclear Medicine* **2017**, *58* (4), 590–597. https://doi.org/10.2967/jnumed.116.182097.

(31) Wang, X.; Gao, S.; Qin, Z.; Tian, R.; Wang, G.; Zhang, X.; Zhu, L.; Chen, X. Evans Blue Derivative-Functionalized Gold Nanorods for Photothermal Therapy-Enhanced Tumor Chemotherapy. *ACS Applied Materials and Interfaces* **2018**, *10* (17), 15140–15149. https://doi.org/10.1021/acsami.8b02195.

(32) Zhou, M.; Luo, Y.; Zeng, W.; Yang, X.; Chen, T.; Zhang, L.; He, X.; Yi, X.; Li, Y.; Yi, X. A Co-Delivery System Based on a Dimeric Prodrug and Star-Shaped Polymeric Prodrug Micelles for Drug Delivery. *Frontiers in Chemistry* **2021**, *9*, 810. https://doi.org/10.3389/FCHEM.2021.765021/.

(33) Salvage, J. P.; Thom, C.; Lewis, A. L.; Phillips, G. J.; Lloyd, A. W. Nanoprecipitation of Polymeric Nanoparticle Micelles Based on 2-Methacryloyloxyethyl Phosphorylcholine (MPC) with 2-(Diisopropylamino)Ethyl Methacrylate (DPA), for Intracellular Delivery Applications. *J Mater Sci Mater Med* **2015**, *26* (3), 150. https://doi.org/10.1007/s10856-015-5480-9.

(34) Gonda, A.; Zhao, N.; Shah, J. V.; Calvelli, H. R.; Kantamneni, H.; Francis, N. L.; Ganapathy, V. Engineering Tumor-Targeting Nanoparticles as Vehicles for Precision Nanomedicine. *Med One* **2019**, *4*, e190021. https://doi.org/10.20900/mo.20190021.

(35) Fucikova, J.; Kepp, O.; Kasikova, L.; Petroni, G.; Yamazaki, T.; Liu, P.; Zhao, L.; Spisek, R.; Kroemer, G.; Galluzzi, L. Detection of Immunogenic Cell Death and Its Relevance for Cancer Therapy. *Cell Death and Disease* **2020**, *11* (11). https://doi.org/10.1038/s41419-020-03221-2.

TABLE OF CONTENT GRAPHIC